Biogeosciences Discuss., doi:10.5194/bg-2016-298, 2016
Manuscript under review for journal Biogeosciences
Published: 2 August 2016

Biogeosciences Discussions
Open Access
EGU

Quantification of multiple simultaneously occurring nitrogen flows in the euphotic ocean

Min Nina Xu[1], Yanhua Wu[2], Li Wei Zheng[1], Zhenzhen Zheng[1], Huade Zhao[3], Edward A Laws[4], Shuh-Ji Kao[1]*

[1]State Key Laboratory of Marine Environmental Science, Xiamen University, Xiamen, China

[2]Shenzhen Marine Environment Monitoring Center Station, Shenzhen, China

[3]National Marine Environmental Monitoring Center, Dalian, China

[4]School of the Coast & Environment, Louisiana State University, USA

Correspondence to: Shuh-Ji Kao (sjkao@xmu.edu.cn)

Biogeosciences Discuss., doi:10.5194/bg-2016-298, 2016
Manuscript under review for journal Biogeosciences
Published: 2 August 2016

12 **Abstract**

13 The general features of the N cycle in the sunlit ocean are known, but quantitative
14 information about multiple transformation rates among nitrogen pools, i.e., ammonium
15 (NH_4^+), nitrite (NO_2^-), nitrate (NO_3^-) and particulate/dissolved organic nitrogen
16 (PN/DON), are limited due to methodological difficulties. By adding a single
17 ^{15}N-labelled NH_4^+ tracer into incubators, we monitored the changes in concentration
18 and isotopic composition of the total dissolved nitrogen (TDN), PN, NH_4^+, NO_2^-, and
19 NO_3^- pools to trace the ^{15}N and ^{14}N flows. Based on mass conservation and isotope
20 mass balance, we formulated a matrix equation that allowed us to simultaneously
21 derive the rates of multiple transformation processes in the nitrogen reaction web. We
22 abandoned inhibitors and minimized the alteration of the system by adding a limited
23 amount of tracer. In one single incubation, solution of the matrix equation provided the
24 rates of NH_4^+, NO_2^-, and NO_3^- uptake; ammonia oxidation; nitrite oxidation; nitrite
25 excretion; DON release; and potentially, the remineralization rate. To our knowledge,
26 this is the first and most convenient method designed to quantitatively and
27 simultaneously resolve complicated nitrogen transformation rates, albeit with some
28 uncertainties. Field examples are given, and comparisons with conventional labeling
29 methods are discussed.

30 **Keywords**

31 Ammonium oxidation, isotope matrix, new production, nitrification, regenerated
32 production

Biogeosciences Discuss., doi:10.5194/bg-2016-298, 2016
Manuscript under review for journal Biogeosciences
Published: 2 August 2016

1. Introduction

Nitrogen (N), which is an essential element in organisms' metabolic processes, regulates productivity as a limiting nutrient in the surface waters of many parts of the ocean (Falkowski, 1997; Zehr and Kudela, 2011; Casciotti, 2016). In the euphotic zone, nitrogen rapidly interconverts among five major N compartments: particulate organic nitrogen (PN), dissolved organic nitrogen (DON), ammonium (NH_4^+), nitrite (NO_2^-), and nitrate (NO_3^-) (Fig. 1 a). Quantitative information on transformation rates in the marine N-cycle may advance our understanding of the coupling of autotrophic and heterotrophic processes involving carbon and nitrogen and the efficiency of the biological pump. Such information would also facilitate evaluation of ecosystem functions. However, the dynamic nature and complexity of the reactions involving nitrogen make it a difficult task to resolve the rates of multiple simultaneous nitrogen transformations. Inventory and isotope tracer methods have often been used in previous studies; however, determining the rate of a specific process is difficult without using inhibitors to block other processes that affect the concentrations of products and reactants, and of course rates of nitrogen transformations are affected by a variety of abiotic conditions (e.g., light and dark; Ward, 2008, 2011 and references therein).

The inventory method is often used to determine the uptake rates of ammonium, nitrite, nitrate, and urea (McCarthy and Eppley, 1972; Harvey and Caperon, 1976; Harrison and Davis, 1977; Dugdale and Wilkerson, 1986; Howard et al., 2007) and to examine the occurrence and rate of nitrification (Wada and Hatton, 1971; Pakulski et al., 1995;

Biogeosciences Discuss., doi:10.5194/bg-2016-298, 2016
Manuscript under review for journal Biogeosciences
Published: 2 August 2016

54 Ward, 2011 and references therein). However, because the concentrations of all forms
55 of nitrogen are affected by multiple processes, inhibitors have typically been added to
56 isolate the effects of specific processes. For example, the concentration of ammonium
57 is simultaneously manily controlled by phytoplankton consumption (PN as the product),
58 nitrifier utilization (nitrite/nitrate as the product), and addition via remineralization
59 from heterotrophic bacterial metabolism, zooplankton excretion, and viral lysis.
60 Therefore, inhibitors (parallel experiments with various inhibitors) have been applied
61 in many studies to block confounding processes (Bianchi et al., 1997; Santoro et al.,
62 2010a; Newell et al., 2011; Ward, 2011; Fernandez and Far ás, 2012; Grundle and
63 Juniper, 2011; Grundle et al., 2013; Martens-Habbena et al., 2015). Unfortunately, the
64 addition of inhibitors may cause undesirable side effects (Ward, 2011; Ward, 2008 and
65 references therein).

66 The ^{15}N-labeled tracer technique has been widely used as a direct measure of specific
67 nitrogen processes since the emergence of isotope ratio mass spectrometry (IRMS). For
68 example, the addition of ^{15}N-labeled nitrate has been applied to estimate new
69 production (Dugdale and Goering, 1967; Chen, 2005; Painter et al., 2014). Likewise, by
70 incubating water to which $^{15}NH_4^+$ has been added under dark and light conditions, rates
71 of nitrification ($^{15}NO_3^-$ as product) have been measured (e.g. Newell et al., 2013; Hsiao
72 et al., 2014; Peng et al., 2016) and rates of ammonium uptake (regenerated production)
73 ($^{15}N_{PN}$) (e.g. Dugdale and Goering, 1967; Dugdale and Wilkerson, 1986; Bronk et al.,
74 1994, 2014). However, ammonium uptake, nitrification, nitrate uptake, and ammonium

Biogeosciences Discuss., doi:10.5194/bg-2016-298, 2016
Manuscript under review for journal Biogeosciences
Published: 2 August 2016

75 excretion occur simultaneously not only in the incubation bottles but also in the field.
76 For instance, Yool et al. (2007) synthesized available global data and indicated that the
77 fractional contribution of nitrate derived from nitrification in the euphotic zone to
78 nitrate uptake can be as high as 25–30%. Unfortunately, nitrate uptake rates were
79 determined under light conditions, and nitrification was determined under dark
80 conditions (Grundle and Juniper, 2011; Grundle et al., 2013), which are not comparable
81 in terms of their effects on these processes. To overcome this problem, 24-h incubation
82 have been used to compensate for the diel cycle of light-sensitive processes (Beman et
83 al., 2012). However, 24-h incubations may cause calculation artifacts due to the
84 interference from significant, multiple transfers of ^{15}N and ^{14}N among pools. An
85 innovative method to simultaneously measure multiple N flows is therefore needed to
86 more realistically resolve nitrogen transformations in the euphotic zone. Marchant et al.
87 (2016) have reviewed recent advances in marine N-cycle studies using ^{15}N-labeling
88 substrates combined with nanoSIMS, FISH, or HISH. These methods provide
89 information about the N cycle at the cellular and molecular level. Nevertheless, the
90 rates of multiple transfers among compartments have not yet been measured
91 simultaneously within a community of microorganisms.

92 In this study, we propose an "isotope matrix method" that is simple in concept. To
93 avoid perturbations, the concentration of the tracer was limited to < 20 % of the
94 substrate concentration, as suggested by previous researchers (Raimbault and Garcia,
95 2008; Middelburg and Nieuwenhuize, 2000; Painter et al., 2014). One single tracer,

Biogeosciences Discuss., doi:10.5194/bg-2016-298, 2016
Manuscript under review for journal Biogeosciences
Published: 2 August 2016

$^{15}NH_4^+$, was added to trace the ^{15}N flows among the nitrogen pools under simulated *in situ* conditions. Almost all well accepted important processes in the N cycle can be quantified with this newly proposed method. To demonstrate the applicability of the method, we conducted incubation experiments in high-nutrient, coastal water off southeastern China and in low-nutrient water in the western North Pacific. We found that the success of the method was determined by the analytical precision of the isotopic ratios of the dissolved pools, especially when concentrations were low. Application of the method was facilitated by advances in the analytical methods used to determine the concentration and isotopic composition of various nitrogen species. Use of the new method allowed us to realistically quantify surface water nitrogen dynamics. The method was also validated using the STELLA model.

2. Isotope matrix method

2.1 Framework of the inter-connections among nitrogen pools

In the oxygenated and well-lit euphotic zone, the transformations of N between NH_4^+, NO_2^-, NO_3^-, PN, and DON, are shown in Fig. 1. PN is operationally defined as the organic nitrogen of particles trapped on a GF/F filter. Dissolved inorganic nitrogen (DIN) and DON are the inorganic and organic nitrogen, respectively, in the dissolved fraction that passes through a polycarbonate membrane with a 0.22 μm pore size. Since DON includes the N in numerous dissolved organic N compounds, including unidentified organics, urea, amino acids, amines, and amides, DON represents the

Biogeosciences Discuss., doi:10.5194/bg-2016-298, 2016
Manuscript under review for journal Biogeosciences
Published: 2 August 2016

116 "bulk" DON and is calculated by subtracting the concentrations of NH_4^+, NO_2^-, and
117 NO_3^- (DIN) from the total dissolved N (TDN).

118 As illustrated by the Michaelis-Menten equation (MacIsaac and Dugdale, 1969), a
119 zero-order reaction is a reaction for which the rate F is constant and independent of the
120 substrate (nitrogen herein) concentration. In other words, the reaction kinetics are
121 substrate-saturated, even when the substrate concentration decreases with time. In
122 contrast, in the nitrogen-poor oligotrophic ocean, the substrate concentration is
123 relatively low, and the reaction is a first-order reaction. In that case, the reaction rate is
124 directly proportional to the substrate concentration; however, the specific rate (k, h^{-1}) is
125 constant. We thus consider two different types of schemes in our method: high nitrogen
126 and low nitrogen (Fig. 1 a and b). Here, we describe the high nitrogen case as an
127 example.

128 The consumption of reactive inorganic nitrogen (NH_4^+, NO_2^-, and NO_3^-) is dominated
129 by photosynthetic uptake by phytoplankton (F_1, F_3, and F_5 in Fig. 1a). Due to DIN
130 assimilation by phytoplankton, the PN pool may increase, but DON (F_8 in Fig. 1a)
131 (Bronk and Glibert, 1993, Bronk et al., 1994; Bronk and Ward, 2000; Varela et al.,
132 2005) and NO_2^- (F_7 in Fig. 1a) may be released (Wada and Hatton, 1971; Collos, 1998;
133 Flynn and Flynn, 1998; Lomas and Lipschultz, 2006) during assimilation. Besides
134 being reduced by phytoplankton uptake, the concentration of NH_4^+ may be increased by
135 remineralization (F_2 in Fig. 1a) and reduced by nitrification. Nitrification consists of

Biogeosciences Discuss., doi:10.5194/bg-2016-298, 2016
Manuscript under review for journal Biogeosciences
Published: 2 August 2016

two basic steps: ammonia oxidation by archaea/bacteria (AOA/AOB) that oxidize ammonia to nitrite (F_4 in Fig. 1a) and nitrite oxidation to nitrate by nitrite-oxidizing bacteria (NOB) (F_6 in Fig. 1a). Note that recent studies have revealed a single microorganism that may completely oxidize NH_4^+ to NO_3^- (comammox) (Daims et al., 2015; van Kessel et al., 2015), but its importance in the marine environment remains unclear. Specific mechanisms or processes such as grazing and viral lysis may also change the concentrations of NH_4^+, nitrite, and DON. However, the scope of this study is to determine the nitrogen flows and exchanges among the often measured and operationally defined pools of nitrogen. In this context, grazers and viruses belong to the operationally defined PN and DON pools, respectively. Thus the roles of processes such as grazing and viral lysis are incorporated in the paradigm depicted in Fig. 1.

The paradigm for the low nutrient case (Fig. 1b) is the same as the paradigm for the high nutrient case, except that we combined NO_2^- and NO_3^- into NO_x^-.

2.2 Analytical methods to determine the amounts of $^{15}N/^{14}N$ in various pools

Our newly proposed method basically couples the ^{15}N-labelling and inventory methods. To trace the ^{15}N movement among pools, changes in the concentration and isotopic composition of the target pools need to be determined. Analytical methods to determine the concentrations and isotopic compositions of both high and low levels of inorganic/organic nitrogen are in most cases well established and have been reported

Biogeosciences Discuss., doi:10.5194/bg-2016-298, 2016
Manuscript under review for journal Biogeosciences
Published: 2 August 2016

155 elsewhere. We determined all of the mentioned concentrations and isotopic
156 compositions except the isotopic composition of NH_4^+.

157 Concentrations of NH_4^+ higher than 0.5 μM were measured manually by using the
158 colorimetric phenol hypochlorite technique (Koroleff, 1983). Nanomolar NH_4^+
159 concentrations were measured by using the fluorometric *o*-phthaldialdehyde (OPA)
160 method (Zhu et al., 2013). Concentrations of NO_2^- and NO_x^- (NO_2^- + NO_3^-) were
161 determined with the chemiluminescence method following the protocol of Braman and
162 Hendrix (1989). The detection limits of NO_2^- and NO_x^- were both ~ 10 nmol L^{-1}, and
163 the corresponding relative precision was better than 5% within the range of
164 concentrations that we measured. By using persulfate as an oxidizing reagent, we
165 oxidized TDN and PN separately to nitrate (Knapp et al., 2005) and then measured the
166 nitrate by using the analytical method for NO_x^- described above.

167 We determined the $\delta^{15}N$ of NO_2^- with the azide method by following the detailed
168 procedures in McIlvin and Altabet (2005). The $\delta^{15}N$ of NO_x^- was determined by using a
169 distinct strain of bacteria that lacked N_2O reductase activity to quantitatively convert
170 NO_x^- to nitrous oxide (N_2O), which we then analyzed by IRMS (denitrifier method;
171 (Sigman et al., 2001; Casciotti et al., 2002). The isotopic composition of NO_3^- was
172 determined from isotope mass balance (NO_x^- minus NO_2^-) or measured by the
173 denitrifier method after eliminating preexisting NO_2^- with sulfamic acid (Granger and
174 Sigman, 2009). To determine the $\delta^{15}N$ of TDN and PN, both species were converted to

Biogeosciences Discuss., doi:10.5194/bg-2016-298, 2016
Manuscript under review for journal Biogeosciences
Published: 2 August 2016

175 NO_3^- with the denitrifier method and the $\delta^{15}N$ of the NO_3^- was determined as described
176 above. The most popular way to determine the N isotopic composition of NH_4^+ is the
177 "diffusion method", which involves conversion of dissolved NH_4^+ to NH_3 gas by
178 raising the sample pH to above 9 with magnesium oxide (MgO) and subsequently
179 trapping the gas quantitatively as $(NH_4)_2SO_4$ on a glass fiber (GF) filter; the isotope
180 ratios of the $^{15}N/^{14}N$ are then measured using a coupled elemental analyzer with an
181 IRMS (Holmes et al., 1998; Hannon and Böhlke, 2008). Alternatively, after removing
182 the preexisting NO_2^- from the seawater samples using sulfanilic acid, NH_4^+ is first
183 quantitatively oxidized to NO_2^- by hypobromite (BrO^-) at pH ~12 (BrO^- oxidation
184 method), and the protocol of McIlvin and Altabet (2005) is then used to reduce the
185 NO_2^- to N_2O (Zhang et al., 2007). Unfortunately, neither of these methods has been
186 established in our lab yet. The isotope matrix method requires the isotopic composition
187 of NH_4^+ as well, but this requirement can be circumvented by making certain
188 assumptions, as illustrated in our case studies.

189 We estimated the amount of ^{14}N and ^{15}N atoms in every individual pool for which we
190 knew the concentration and $\delta^{15}N$. By assuming the ^{15}N content of standard atmospheric
191 nitrogen to be 0.365%, we used the $\delta^{15}N$ of each sample and Eq. (1) to calculate R_{sample}
192 ($^{15}N/^{14}N$). By defining r_{sample} as $^{15}N/(^{14}N+^{15}N)$ in Eq. (2), we derived the ^{15}N and ^{14}N
193 concentrations of all forms of N through Eqs. (3) and (4), with the exception of NH_4^+
194 and DON. The r value of the NH_4^+ was assumed to equal either its initial value or an
195 arbitrarily chosen fraction thereof, and the ^{15}N and ^{14}N content of the the NH_4^+ was then

Biogeosciences Discuss., doi:10.5194/bg-2016-298, 2016
Manuscript under review for journal Biogeosciences
Published: 2 August 2016

196 determined using Eqs. (3) and (4). The ^{15}N and ^{14}N concent of the DON was then
197 determined by mass balance (N_2 fixation and emission of nitrogenous gases were
198 ignored).

199 $$\delta^{15}N\left(‰ vs.air\right)=\left[\frac{\left(\frac{^{15}N}{^{14}N}\right)_{sample}}{\left(\frac{^{15}N}{^{14}N}\right)_{air}}-1\right]\times 1000 \quad (1)$$

200 $$r=\frac{^{15}N}{^{15}N+^{14}N}=\frac{\frac{^{15}N}{^{14}N}}{\frac{^{15}N}{^{14}N}+1} \quad (2)$$

201 $$\left[^{15}N\right]=\left[N\right]\times r \quad (3)$$

202 $$\left[^{14}N\right]=\left[N\right]\times(1-r) \quad (4)$$

203 **2.3 Formation of matrix equations**

204 Isotopic mass balance of the incubation system at every point in time was thus achieved.
205 In other words, the sums of the variations in the total N, ^{15}N, and ^{14}N concentrations
206 were zero, as shown in Eqs. (5–7).

207 $$\Delta\left[NH_4^+\right]+\Delta\left[NO_2^-\right]+\Delta\left[NO_3^-\right]+\Delta\left[PN\right]+\Delta\left[DON\right]=0 \quad (5)$$

208 $$\Delta\left[^{15}NH_4^+\right]+\Delta\left[^{15}NO_2^-\right]+\Delta\left[^{15}NO_3^-\right]+\Delta\left[^{15}\text{N-PN}\right]+\Delta\left[^{15}\text{N-DON}\right]=0 \quad (6)$$

209 $$\Delta\left[^{14}NH_4^+\right]+\Delta\left[^{14}NO_2^-\right]+\Delta\left[^{14}NO_3^-\right]+\Delta\left[^{14}\text{N-PN}\right]+\Delta\left[^{14}\text{N-DON}\right]=0 \quad (7)$$

Biogeosciences Discuss., doi:10.5194/bg-2016-298, 2016
Manuscript under review for journal Biogeosciences
Published: 2 August 2016

In this newly proposed method, we added a tracer amount of $^{15}NH_4^+$ into the incubation system at the very beginning and then monitored the changes of ^{15}N and ^{14}N in the five pools. Subsamples were collected for analysis (at times of 0, 1.6, 4.4, 8.8, and 14.6 h in high nutrient case and 0, 4.3, 11.8 and 23.7 in low nutrient case) after the start of the experiment. We assumed no fractionation between ^{15}N and ^{14}N for all the transfer reactions among the pools. The fluxes of ^{15}N and ^{14}N were therefore assumed to equal the total flux multiplied by $r_{substrate}$ and $(1 - r_{substrate})$, respectively. Isotope fractionation could easily be introduced into the equations if necessary, i.e. dividing ^{14}N flux by α (the ratio of specific rate constant of ^{14}N to ^{15}N), and the flux of ^{15}N is obtained. In the zero-order reaction scheme, the fluxes remain unchanged through time; however, the r values for different pools may vary significantly due to the redistribution of the ^{15}N tracer. According to mass balance, the changes of the ^{15}N concentrations of the NH_4^+, NO_2^-, NO_3^-, and (PN + DON) pools over time are determined by the inflow and outflow of ^{15}N, as shown by Eqs. (8–11), respectively. Because the DON release rate (F_8) is deduced from mass conservation, it is inappropriate to add the DON pool in the matrix as an independent equation. Similarly, the temporal dependence of ^{14}N-NH_4^+, ^{14}N-NO_2^-, ^{14}N-NO_3^- and ^{14}N-(PN+DON) were expressed by Eqs. (12–15), respectively.

$$\frac{d\left[{}^{15}NH_4^+\right]}{dt} = F_2 \times r_{PN} - (F_1 + F_4) \times r_{NH_4^+} \quad (8)$$

Biogeosciences Discuss., doi:10.5194/bg-2016-298, 2016
Manuscript under review for journal Biogeosciences
Published: 2 August 2016

$$\frac{\mathrm{d}\left[{}^{15}\mathrm{NO_2^-}\right]}{\mathrm{dt}} = F_4 \times r_{NH_4^+} + F_7 \times r_{PN} - (F_3 + F_6) \times r_{NO_2^-} \quad (9)$$

$$\frac{\mathrm{d}\left[{}^{15}\mathrm{NO_3^-}\right]}{\mathrm{dt}} = F_6 \times r_{NO_2^-} - F_5 \times r_{NO_3^-} \quad (10)$$

$$\frac{\mathrm{d}\left[{}^{15}\text{N-PN}\right]}{\mathrm{dt}} + \frac{\mathrm{d}\left[{}^{15}\text{N-DON}\right]}{\mathrm{dt}} = F_1 \times r_{NH_4^+} + F_3 \times r_{NO_2^-} + F_5 \times r_{NO_3^-} - F_2 \times r_{PN} - F_7 \times r_{PN} \quad (11)$$

$$\frac{\mathrm{d}\left[{}^{14}\mathrm{NH_4^+}\right]}{\mathrm{dt}} = F_2 \times (1 - r_{PN}) - (F_1 + F_4) \times (1 - r_{NH_4^+}) \quad (12)$$

$$\frac{\mathrm{d}\left[{}^{14}\mathrm{NO_2^-}\right]}{\mathrm{dt}} = F_4 \times (1 - r_{NH_4^+}) + F_7 \times (1 - r_{PN}) - (F_3 + F_6) \times (1 - r_{NO_2^-}) \quad (13)$$

$$\frac{\mathrm{d}\left[{}^{14}\mathrm{NO_3^-}\right]}{\mathrm{dt}} = F_6 \times (1 - r_{NO_2^-}) - F_5 \times (1 - r_{NO_3^-}) \quad (14)$$

$$\frac{\mathrm{d}\left[{}^{14}\text{N-PN}\right]}{\mathrm{dt}} + \frac{\mathrm{d}\left[{}^{14}\text{N-DON}\right]}{\mathrm{dt}} = F_1 \times (1 - r_{NH_4^+}) + F_3 \times (1 - r_{NO_2^-}) + F_5 \times (1 - r_{NO_3^-}) - F_2 \times (1 - r_{PN}) - F_7 \times (1 - r_{PN}) \quad (15)$$

We solved Eqs. (8–15) for the fluxes F_1 through F_7 during the first two hours of the experiment with the following matrix equation:

Biogeosciences Discuss., doi:10.5194/bg-2016-298, 2016
Manuscript under review for journal Biogeosciences
Published: 2 August 2016

$$\begin{pmatrix} -r_{NH_4^+} & r_{PN} & 0 & -r_{NH_4^+} & 0 & 0 & 0 \\ 0 & 0 & -r_{NO_2^-} & r_{NH_4^+} & 0 & -r_{NO_2^-} & r_{PN} \\ 0 & 0 & 0 & 0 & -r_{NO_3^-} & r_{NO_2^-} & 0 \\ r_{NH_4^+} & -r_{PN} & r_{NO_2^-} & 0 & r_{NO_3^-} & 0 & -r_{PN} \\ -(1-r_{NH_4^+}) & (1-r_{PN}) & 0 & -(1-r_{NH_4^+}) & 0 & 0 & 0 \\ 0 & 0 & -(1-r_{NO_2^-}) & (1-r_{NH_4^+}) & 0 & -(1-r_{NO_2^-}) & (1-r_{PN}) \\ 0 & 0 & 0 & 0 & -(1-r_{NO_3^-}) & (1-r_{NO_2^-}) & 0 \\ (1-r_{NH_4^+}) & -(1-r_{PN}) & (1-r_{NO_2^-}) & 0 & (1-r_{NO_3^-}) & 0 & -(1-r_{PN}) \end{pmatrix} \times \begin{pmatrix} F_1 \\ F_2 \\ F_3 \\ F_4 \\ F_5 \\ F_6 \\ F_7 \end{pmatrix} = \begin{pmatrix} \frac{d[^{15}NH_4^+]}{dt} \\ \frac{d[^{15}NO_2^-]}{dt} \\ \frac{d[^{15}NO_3^-]}{dt} \\ \frac{d[^{15}\text{N-PN}]}{dt} + \frac{d[^{15}\text{N-DON}]}{dt} \\ \frac{d[^{14}NH_4^+]}{dt} \\ \frac{d[^{14}NO_2^-]}{dt} \\ \frac{d[^{14}NO_3^-]}{dt} \\ \frac{d[^{14}\text{N-PN}]}{dt} + \frac{d[^{14}\text{N-DON}]}{dt} \end{pmatrix} \quad (16)$$

The rates of change of the N concentrations were approximated by one-sided finite difference expressions. For example, $d[^{14}NH_4^+]/dt$ at time t = 0 was appxoximated by $\{[^{14}NH_4^+]_{t1} - [^{14}NH_4^+]_{t0}\}/2$ where the subscripts indicate the times at which the concentrations were measured. Given these estimates of the derivatives on the right-hand side of Eq. (16), we solved for the fluxes F_1 through F_7 during the first two hours by assuming that the r values were equal to the average of the r values at times 0 and 2 hours. The flux F_8 was then determined by conservation of mass.

Unlike the high-nitrogen case, the reaction rate (k_i*C) changed over time as a result of changes of the substrate concentration in the low-nitrogen scenario (Fig. 1b). The relevant equations in that case are Eqs. (8–15). In this case nitrite and nitrate were combined into one pool (NO_x^-). The total number of equations was therefore reduced from eight to six. Meanwhile, $r_{substrate}$, $1 - r_{substrate}$ and F_i were replaced by $[^{15}N]$, $[^{14}N]$

Biogeosciences Discuss., doi:10.5194/bg-2016-298, 2016
Manuscript under review for journal Biogeosciences
Published: 2 August 2016

and k_i, respectively. Eq. (17) is the matrix form of the equations. Because in this case the first-order reaction rates varied rapidly, short-term incubation data were especially appropriate for calculating k_i values. In solving Eq. (17) for the rate constants during the first two hours of the experiment, we equated the ^{14}N and ^{15}N concentrations in the left-hand matrix to the averages of the corresponding concentrations at t0 and t1.

$$\begin{pmatrix} -\left[{}^{15}NH_4^+\right] & \left[{}^{15}N\text{-}PN\right] & -\left[{}^{15}NH_4^+\right] & 0 & 0 \\ 0 & 0 & \left[{}^{15}NH_4^+\right] & -\left[{}^{15}NO_X^-\right] & \left[{}^{15}N\text{-}PN\right] \\ \left[{}^{15}NH_4^+\right] & -\left[{}^{15}N\text{-}PN\right] & 0 & \left[{}^{15}NO_X^-\right] & -\left[{}^{15}N\text{-}PN\right] \\ -\left[{}^{14}NH_4^+\right] & \left[{}^{14}N\text{-}PN\right] & -\left[{}^{14}NH_4^+\right] & 0 & 0 \\ 0 & 0 & \left[{}^{14}NH_4^+\right] & -\left[{}^{14}NO_X^-\right] & \left[{}^{14}N\text{-}PN\right] \\ \left[{}^{14}NH_4^+\right] & -\left[{}^{14}N\text{-}PN\right] & 0 & \left[{}^{14}NO_X^-\right] & -\left[{}^{14}N\text{-}PN\right] \end{pmatrix} \times \begin{pmatrix} k_1 \\ k_2 \\ k_3 \\ k_4 \\ k_5 \end{pmatrix} = \begin{pmatrix} \frac{d\left[{}^{15}NH_4^+\right]}{dt} \\ \frac{d\left[{}^{15}NO_X^-\right]}{dt} \\ \frac{d\left[{}^{15}N\text{-}PN\right]}{dt} + \frac{d\left[{}^{15}N\text{-}DON\right]}{dt} \\ \frac{d\left[{}^{14}NH_4^+\right]}{dt} \\ \frac{d\left[{}^{14}NO_X^-\right]}{dt} \\ \frac{d\left[{}^{14}N\text{-}PN\right]}{dt} + \frac{d\left[{}^{14}N\text{-}DON\right]}{dt} \end{pmatrix} \quad (17)$$

2.4 Validation by Stella

Because the matrix equations provide approximate solutions, we used STELLA 9.1.4 software (Isee systems, Inc.) to construct models that were consistent with the scenarios depicted in Fig. 1 to simulate, as accurately as possible, the continuous fluxes of nitrogen and to thus check the applicability of the isotope matrix method to analysis of the observational data. The model was divided into two modules, one for ^{15}N and the other for ^{14}N. The modules balanced the total amounts of these isotopes in the NH_4^+, NO_2^-, NO_3^- (or NO_x^-), PN, and DON pools. The connection between these two modules was through the ^{15}N atom % (r_N). The pool size was regulated by the F or k

Biogeosciences Discuss., doi:10.5194/bg-2016-298, 2016
Manuscript under review for journal Biogeosciences
Published: 2 August 2016

values derived from solution of the matrix equations during the first two hours of the experiments (Fig. S1 and S2). After setting the initial concentrations of ^{15}N and ^{14}N to that measured in every pool, the model was run for 24 h according to the short-term F (1.6 h) or k (4.3 h) values derived from the matrix equations. The model outputs of the two cases are presented below. The output includes the time courses of the ^{15}N and ^{14}N concentrations and the ^{15}N atom% (r_N) or $\delta^{15}N$ of each N species. Through this comparison, we could observe the evolution of the isotopic composition in the various N pools.

In our case study, we measured all isotopic compositions, except that of NH_4^+. In the cases presented below, we fixed the isotopic composition of NH_4^+ for the first model run, i.e., no remineralization. This assumption has been made in many previous studies (e.g. Dugdale and Goering, 1967; Ward et al., 1984; Santoro et al., 2010a, Santoro et al., 2013; Hsiao et al., 2014; Peng et al., 2015). However, the assumption has been criticised based on the fact that the labeled ammonium pool can be diluted by regenerated ammonium (e.g. Caperon et al., 1979; Blackburn, 1979; Gilbert et al., 1982; Dugdale and Wilkerson, 1986; Kanda et al., 1987; Dickson and Wheeler, 1995; Clark et al., 2006; Raimbault and Garcia, 2008). The ammonium excretion rates calculated with these dilution models, however, have been based on some assumptions. Examples of these assumptions have included the following: (1) the uptake and excretion rates remain constant during the incubation, (2) no ^{15}N is excreted, and (3) PN concentrations change insignificantly. In addition, the amounts of $^{15}NH_4^+$ that needed to be added have

Biogeosciences Discuss., doi:10.5194/bg-2016-298, 2016
Manuscript under review for journal Biogeosciences
Published: 2 August 2016

291 sometimes been greater than the ambient concentration, depending on the number of
292 trophic levels in the system (Caperon et al., 1979; Blackburn, 1979; Kanda et al., 1987).
293 All of the models have assumed that PON was the only sink of ^{15}N. These studies have
294 broadened our insight into NH_4^+ cycling, even though they have made arbitrary
295 assumptions and considered only NH_4^+ excretion and incorporation into PN. To test the
296 validity of the assumption of insignificant NH_4^+ excretion in our cases, we activated
297 remineralization to various degrees in the model runs. We also compared the observed
298 and remineralization-associated simulations.

299 **3. High-nutrient case in a coastal bay in southern China**

300 **3.1 Study site and environmental data**

301 Wuyuanwan (WYW), located at the southern coast of China, is an inner bay with a
302 regular semidiurnal tide. Its water flows out during neap tide, and water from the open
303 ocean flows into the bay during spring tide. The water is well ventilated and constantly
304 saturated with dissolved oxygen. As a coastal bay, Wuyuanwan suffers from
305 anthropogenic influences that result in high nutrient concentrations analogous to other
306 coastal zones in China. It is an ideal research site to study the dynamic transformation
307 processes of the coastal nitrogen cycle.

308 During our sampling (January 2014), the water was vertically well mixed, with a
309 temperature of ~13.7 °C, a salinity of approximately 29.5, and pH of 8.1–8.3. The
310 concentrations of nitrogenous species were relatively high in this highly eutrophic

Biogeosciences Discuss., doi:10.5194/bg-2016-298, 2016
Manuscript under review for journal Biogeosciences
Published: 2 August 2016

311 aquatic system, with inorganic nutrient concentrations of 30.9 ± 0.7 μmol L^{-1} for NO_3^-,
312 22.3 ± 4.3 μmol L^{-1} for NH_4^+, 5.5 ± 0.1 μmol L^{-1} for NO_2^-, and 8.5 ± 0.2 μmol L^{-1} for
313 PN.

314 **3.2 Incubation experiments**

315 Water samples were collected in two pre-washed 10-L polycarbonate bottles (Nalgene,
316 USA). The sampling depth was 0.3 m, with a light intensity of 80 % of the surface water
317 irradiance. ^{15}N-labeled NH_4Cl (98 atom % ^{15}N, Sigma-Aldrich, USA) was added to the
318 incubation bottles (< 10 % of the ambient concentration). The incubations were carried
319 out immediately in an incubator equipped with a light screen allowing 80% light
320 penetration. The temperature was maintained at ~13.7 °C using continuously pumped
321 seawater. The first sample (t_0) was taken immediately after adding the tracer.
322 Subsequent samples were taken at approximately 2–4 h intervals. An aliquot of 200 mL
323 was filtered through a 47-mm polycarbonate membrane with a 0.22 μm pore size
324 (Millipore, USA), and the filtrates were frozen at –20 °C for chemical analysis in the
325 lab. Particulate matter was collected by filtering seawater through pre-combusted
326 (450 °C for 4 h) GF/F filters that were 25 mm in diameter (Whatman, GE Healthcare,
327 USA), under a pressure of <100 mm Hg. The GF/F filters were freeze-dried and stored
328 in a desiccator for further analyses of the PN concentration and isotopes. We selected
329 the first 16 hours for presentation here.

330 **3.3 Results**

Biogeosciences Discuss., doi:10.5194/bg-2016-298, 2016
Manuscript under review for journal Biogeosciences
Published: 2 August 2016

331 **3.3.1 Observational results**

332 The concentrations, nitrogen isotope signatures, ^{15}N atom percentages, and ^{15}N and ^{14}N
333 concentrations of NH_4^+, NO_2^-, NO_3^-, PN, and DON in the incubation showed
334 distinctive patterns along with the incubation time (Fig. 2). The concentrations of NH_4^+
335 and NO_3^- were higher than those of NO_2^-, PN, and DON. NH_4^+ significantly and
336 continuously decreased from 26.6 to 16.5 μmol L^{-1} at a rate of 0.63 μmol L^{-1} h^{-1} over
337 the course of the incubation (Fig. 2a). NO_3^- decreased from 30.9 to 28.3 μmol L^{-1} at a
338 rate of approximately one-third the rate of NH_4^+ (Fig. 2c). The NO_2^- concentration
339 displayed a slightly declining trend (Fig. 2b). Conversely, the PN and DON
340 concentrations steadily increased. The PN concentration increased from 8.8 to 18.3
341 μmol L^{-1} at a rate of 0.66 μmol L^{-1} h^{-1}, which was very close to that of NH_4^+ (Fig. 2d).
342 The DON concentration increased from 17.4 to 20.9 μmol L^{-1} at a rate of 0.22 μmol L^{-1}
343 h^{-1} (Fig. 2e).

344 The time courses of the nitrogen isotopic compositions of NH_4^+, NO_2^-, NO_3^-, PN and
345 DON in the incubation are shown in Figs 2 f–j. The $\delta^{15}N$-NH_4^+ value remained constant
346 without considering NH_4^+ regeneration (Fig. 2f), and $\delta^{15}N$-NO_2^- increased from –9.0 to
347 12.1 ‰ (Fig. 2g); $\delta^{15}N$-NO_3^- ranged from 6.9 to 9.9 ‰ with no significant trend over
348 time (Fig. 2h). In addition, $\delta^{15}N$-PN increased from 14.8 to 2718.8 ‰ (Fig. 2i). Based
349 on the N mass and isotope balance, the calculated value of $\delta^{15}N$-DON followed the
350 same trend as $\delta^{15}N$-PN, increasing from 5.0 to 2617.6 ‰ (Fig. 2j). According to the
351 $\delta^{15}N$ values of these N pools, the ^{15}N atom percentages (r_N) were calculated; they

Biogeosciences Discuss., doi:10.5194/bg-2016-298, 2016
Manuscript under review for journal Biogeosciences
Published: 2 August 2016

displayed a similar pattern as the corresponding $\delta^{15}N$ variation (Figs. 2 k–o). The r values of NO_2^- and NO_3^- varied within narrow ranges (0.36–0.37 %), ten times less than those of NH_4^+, PN, and DON.

The ^{15}N and ^{14}N concentrations of NH_4^+, NO_2^-, NO_3^-, PN, and DON were computed (Figs. 2 p–y) based on their bulk concentrations and ^{15}N atom percentages (r_N). The ^{15}N-NH_4^+ and ^{14}N-NH_4^+ concentrations decreased significantly (Figs. 2 p and u) at rates of 0.026 and 0.61 μmol L^{-1} h^{-1}, respectively. The ^{15}N-NO_2^- and ^{15}N-NO_3^- concentrations varied within relatively small ranges from 0.020 to 0.019 μmol L^{-1} and from 0.11 to 0.10 μmol L^{-1}, respectively (Figs. 2 q and r). The ^{14}N-NO_2^- and ^{14}N-NO_3^- concentrations declined significantly (Figs. 2 v and w) compared with the ^{15}N-NO_2^- and ^{15}N-NO_3^- concentrations. In contrast, the ^{15}N-PN and ^{14}N-PN concentrations increased remarkably (Figs. 2 s and x); the ^{15}N-DON and ^{14}N-DON concentrations exhibited increasing trends similar to that of PN (Figs. 2 t and y). In fact, many of the previous incubation studies observed a significant nitrogen imbalance that was attributed to DON release, reaching an average of ~10–45% (e.g. Dugdale and Wilkerson, 1986; Ward and Bronk, 2001; Bronk and Ward, 1999, 2005; Varela et al., 2005). This magnitude of DON release is in line with our incubation results.

3.3.2 Solutions of the matrix equation and STELLA back calculation

As presented above, the bulk, ^{15}N and ^{14}N concentrations of NH_4^+, NO_2^-, NO_3^-, PN, and DON varied linearly with incubation time, indicating that the reactions in the

Biogeosciences Discuss., doi:10.5194/bg-2016-298, 2016
Manuscript under review for journal Biogeosciences
Published: 2 August 2016

372 incubation system could be treated as a zero-order reaction. We selected the first
373 sampling interval for the calculation of rate constants, although the incubation was
374 conducted for 14.6 h. The r values (NH_4^+, NO_2^-, NO_3^-, and PN) used for computation
375 were the average values of the corresponding pool in the first incubation interval. The
376 results under the assumption of fixed r_{NH4+} conditions are shown in Table 1. The NH_4^+
377 uptake rate (F_1), 0.63 μmol L^{-1} h^{-1}, was much higher than the other rates and followed
378 by the NO_3^- uptake rate (F_5, 0.22 μmol L^{-1} h^{-1}) and DON release rate (F_8, 0.25 μmol L^{-1}
379 h^{-1}). The NO_2^- uptake (F_3) rate was 0.032 μmol L^{-1} h^{-1}, much lower than that of NH_4^+
380 and NO_3^- uptake. The ammonia oxidation rate (F_4) was 0.00090 μmol L^{-1} h^{-1}, but the
381 nitrite oxidation rate (F_6) was undetectable. Since the incubation was conducted under
382 80 % light conditions, low rates of ammonium and nitrite oxidation were reasonable
383 because either nitrifiers and NOB are sensitive to light (e.g. Olson, 1981a, 1981b;
384 Horrigan et al., 1981; Ward, 2005; Merbt et al., 2012). In addition, the nitrification rates
385 may have been constrained by competition with phytoplankton for ammonium under
386 the relatively strong light field (Smith et al., 2014). The nitrite release rate by
387 phytoplankton (F_7) was nearly zero. Similarly, nitrite release was below the limit of
388 detection in Monterey Bay observed by Santoro et al (Santoro et al., 2013).

389 By introducing the measured initial ^{15}N and ^{14}N concentrations of NH_4^+, NO_2^-, NO_3^-,
390 PN, and DON and the calculated rates (F_1–F_8) into the STELLA model (Fig. S1), we
391 obtained successive variations of ^{15}N and ^{14}N concentrations and r_N of NH_4^+, NO_2^-,
392 NO_3^-, PN, and DON over time (Figs. 3 a–o). The model output of the $\delta^{15}N$ values and

Biogeosciences Discuss., doi:10.5194/bg-2016-298, 2016
Manuscript under review for journal Biogeosciences
Published: 2 August 2016

393 bulk N concentrations of these N species could thus be derived (Figs. 3 p–y). The
394 modeled and measured values remained consistent throughout the incubation.

395 To test the effect of regeneration (i.e., activating regeneration and F_2 >0), we allowed
396 r_{NH4+} to decrease to different degrees (1%, 10%, 20%, and 50% of the total at the end of
397 the incubation). As indicated in previous studies, such regeneration-induced isotope
398 dilution indeed altered the original results (Fig. 3). Since ammonium uptake is the
399 dominant process, the alteration of the PN pool was more significant in comparison
400 with the other pools (Figs. 3 d, n and s). To maintain a constant reduction of the
401 measured NH_4^+ concentration, F_1 increased as F_2 increased (Table 1). As the
402 regeneration increased, the deviation of the time course of ^{15}N-PN production (Fig. 3c)
403 increased, resulting in a larger curvature of r-PN and δ^{15}N-PN, and the turning point
404 appeared earlier. This model exercise confirmed the influence of the isotope dilution
405 effect; however, this effect is insignificant in the very early stage of an incubation. Such
406 a result suggests that a better result can be obtained in a short-term incubation only
407 when regeneration is intensive. Nevertheless, the matrix solution fit well with the
408 model run with fixed r-NH_4^+, suggesting that the assumption of no regeneration was
409 plausible, at least in our case during the incubation period.

410 **4. Low-nutrient case in the western North Pacific (WNP)**

411 **4.1 Sampling station and incubation experiment**

Biogeosciences Discuss., doi:10.5194/bg-2016-298, 2016
Manuscript under review for journal Biogeosciences
Published: 2 August 2016

412 The WNP cruise took place from 30 March to 5 May in 2015 aboard the R/V
413 Dongfanghong 2. The survey area covered 25 to 32° N and 120 to 152° E.

414 The station for the experiment was located at 32°37.838′ N and 145°56.759′ E, and
415 water samples were collected using a 24-bottle rosette sampler. The sampling depth
416 was 25 m with relatively low light intensity. Pre-washed 10-L polycarbonate carboys
417 (Nalgene, USA) were used for the incubation. A total 1.5 mL of 200 μM ^{15}N-labelled
418 NH_4Cl tracers containing 98 atom% ^{15}N (Sigma-Aldrich, USA) was injected into the
419 incubation bottle to achieve a final concentration of 30 nM. Incubation was carried out
420 immediately in a thermostatic incubator (GXZ-250A, Ningbo) with a constant light
421 intensity in 33 % level (300 Lux on average) at 18.4 °C, the same as the *in situ* sampling
422 temperature.

423 **4.2 Results**

424 **4.2.1 Observational results**

425 The patterns of the variations of the bulk N concentration, nitrogen isotope signature,
426 ^{15}N atom percentage, and ^{15}N and ^{14}N concentrations of the NH_4^+, NO_x^-, PN, and DON
427 during the incubation are shown in Fig. 4. DON was the dominant N pool (several tens
428 of times higher than NH_4^+, NO_x^-, and PN). NH_4^+ and NO_x^- decreased rapidly at the
429 early stage and later more slowly, dropping from 142.7 to 48.1 nM and 520.7 to 126.8
430 nM, respectively (Figs. 4 a and b). In contrast, PN and DON continuously increased.

Biogeosciences Discuss., doi:10.5194/bg-2016-298, 2016
Manuscript under review for journal Biogeosciences
Published: 2 August 2016

431 The PN concentration increased from 436.8 to 667.0 nM (Fig. 4c), and the DON
432 concentration increased from 5.4 to 5.6 μM (Fig. 4d).

433 Opposite to the trend of NO_x^- concentrations, $\delta^{15}N\text{-}NO_x^-$ increased from 8.9 to 170.6 ‰
434 (Fig. 4f). In addition, $\delta^{15}N$-PN exhibited great changes, increasing from 47 to 6948 ‰
435 (Fig. 4g). Based on the N mass and isotope balance, the calculated $\delta^{15}N$-DON generally
436 showed an increasing trend from 5.0 to 150.1 ‰ that was quite rapid in the beginning
437 and later became steady (Fig. 4h). The variation of ^{15}N atom percentage (r_N) presented a
438 very similar, but not as significant, trend as the corresponding $\delta^{15}N$ variation of specific
439 N species (Figs. 4 i–l). The r values of NO_x^- and DON varied over a narrow range from
440 0.36 to 0.42% (Figs 4 j and l), and r_{PN} increased from 0.38 to 2.83 % (Fig. 4k).

441 The ^{15}N and ^{14}N concentrations of NH_4^+, NO_x^-, PN, and DON (Figs. 4 m–t) were
442 computed, and their trends over time resembled the corresponding bulk concentration
443 changes. The $^{15}N\text{-}NH_4^+$ and $^{14}N\text{-}NH_4^+$ concentrations decreased from 29.8 to 10.0 nM
444 and from 112.9 to 38.0 nM, respectively (Figs. 4 m and q). The $^{15}N\text{-}NO_x^-$ declined from
445 1.9 to 0.5 nM, and $^{14}N\text{-}NO_x^-$ decreased from 518.8 to 126.3 nM (Figs. 4 n and r). In
446 contrast, the ^{15}N-PN and ^{14}N-PN concentrations increased notably from 1.7 to 18.9 nM
447 and 435.1 to 648.1 nM, respectively (Figs. 4 o and s). The ^{15}N and ^{14}N concentrations of
448 DON showed an increasing trend similar to that of PN, ranging from 19.8 to 23.7 nM
449 and from 5.4 to 5.6 μM, respectively (Figs 4 p and t).

450 **4.2.2 Solutions of the matrix equation and STELLA back calculation**

Biogeosciences Discuss., doi:10.5194/bg-2016-298, 2016
Manuscript under review for journal Biogeosciences
Published: 2 August 2016

451 The temporal variations of the bulk, ^{15}N, and ^{14}N concentrations of NH_4^+, NO_x^-, PN,
452 and DON with incubation time revealed patterns of exponential decrease or increase
453 (Fig. 4), demonstrating that the reactions in this low-nutrient system could be treated as
454 first-order reactions. As first-order reactions, the specific rates were fixed. Here, we
455 chose the first sampling interval, i.e., 4.3 h, for the specific rate calculation. The ^{15}N and
456 ^{14}N concentrations of NH_4^+, NO_x^-, and PN for matrix computation were the mean
457 values for the specific time interval.

458 The results under the assumption of constant r_{NH4+} are shown in Table 2. The NO_x^-
459 specific uptake rate (k_4) was 0.059 h^{-1} (27.12 nmol L^{-1} h^{-1}), the highest among these
460 reaction rates, followed by the NH_4^+ specific uptake rate (k_1, 0.045 h^{-1}) and nitrification
461 specific rate (k_3, 0.00050 h^{-1}). The specific rate of the release of NO_2^- by phytoplankton
462 (k_5) was undetectable, similar to a previous report by Santoro et al. (2013), who
463 suggested that phytoplankton NO_2^- excretion may only occur under Fe-limited
464 conditions or when phytoplankton rely on a single N source.

465 By introducing the measured initial ^{15}N and ^{14}N concentrations of NH_4^+, NO_x^-, PN, and
466 DON and the calculated specific rates (k_1 to k_5) into STELLA (Fig. S2), we obtained
467 consecutive changes in all parameters (see Fig. 5). Generally, the model outputs fit well
468 with the measured values, except for the ^{15}N concentration, $\delta^{15}N$, and r_N of PN, for
469 which the last data points were slightly higher than the model (Figs. 5 c, k and o). Since
470 this case was conducted under low-nutrient conditions, this positive offset was

Biogeosciences Discuss., doi:10.5194/bg-2016-298, 2016
Manuscript under review for journal Biogeosciences
Published: 2 August 2016

probably compensated for by organic nitrogen utilization. The low level of nitrate and ammonium, in fact, was approaching the concentration threshold for phytoplankton utilization (e.g., <30–40 nM NH_4^+ for *Emiliania huxleyi*; Sunda and Ransom, 2007). Our flow cytometry data demonstrated that the growth of eukaryotes was slowing down, but the growth of *Synechococcus* was continuous (not shown). In general, the system followed a first-order reaction in the first 16 hours, and this simulation demonstrated the applicability of this matrix method.

In order to test the validity of the assumption of no regeneration, r_{NH4+} was artificially decreased by 1 %, 10 %, 20 %, and 50 % in total by the end of the incubation (a span of 23.7 h). The experiment was conducted in the same way as the high-nutrient case, and the results are shown in Table 2 and Fig. 5. The specific NH_4^+ uptake rate (k_1) increased as the regeneration (k_2) increased (Table 2). This resut demonstrated that the effect of r_{NH4+} on NO_x^--associated parameters was trivial (Figs. 5 b, f, j, n, and r). In contrast, the variation of NH_4^+ regeneration significantly affected the ^{15}N concentration, $\delta^{15}N$, and r_N of PN. More specifically, greater NH_4^+ regeneration resulted in larger differences between these three PN-associated values and the STELLA-modeled data (Figs. 5 c, k and o). Thus, the NH_4^+ regeneration rate could be ignored, at least in the early stage in our case, a reflection of the good agreement with the model run.

5. Comparisons with traditional methods

Biogeosciences Discuss., doi:10.5194/bg-2016-298, 2016
Manuscript under review for journal Biogeosciences
Published: 2 August 2016

490 Below, we present a comparison with conventional rate measurements of ammonium
491 oxidation and uptake. The most popular N uptake rate calculation (i.e. Eq. (18)) follows
492 Dugdale and Wilkerson (1986), and similarly, the calculation of ammonium oxidation
493 in Eq. (19):

494 $$\rho_{NH_4^+} = \frac{(r_t - r_0) \times [PN]_t}{(r_{NH_4^+} - r_0) \times T}, \quad (18)$$

495 $$\rho_{NR} = \frac{(r_t - r_0) \times [NO_X^-]_t}{(r_{NH_4^+} - r_0) \times T}, \quad (19)$$

496 where ρ_{NH4+} (ρ_{NR}) stands for the NH_4^+ assimilation (oxidation) rate; r_0 and r_t
497 represent the initial and final ^{15}N atom %, respectively, in the PN (NO_2^-/NO_x^-) pool;
498 r_{NH4+} is the initial ^{15}N atom % of NH_4^+; $[PN]_t$ ($[NO_x^-]$) represents the final PN ($[NO_x^-]$)
499 concentration; and T is the incubation time in hours.

500 The end products in the above equations, in fact, were also influenced by non-target
501 processes. For example, the DON release (regardless of its cause) was not considered
502 in the canonical method for ammonium uptake (Eq. (18) considers only the ^{15}N
503 retained in particulate pool). In Table 3, the NH_4^+ uptake rate calculated by the matrix
504 method (632.2 nmol L^{-1} h^{-1}) was ~53 % higher than the rate calculated by the
505 traditional method (413.6 nmol L^{-1} h^{-1}) for the high-nutrient case in WYW. In the
506 low-nutrient case, the matrix-derived NH_4^+ uptake rate (4.58 nmol L^{-1} h^{-1}) was ~20 %
507 higher than that (3.86 nmol L^{-1} h^{-1}) from the traditional method. The higher uptake rates
508 were mainly due to the DON release, which was not counted in the traditional method.

Biogeosciences Discuss., doi:10.5194/bg-2016-298, 2016
Manuscript under review for journal Biogeosciences
Published: 2 August 2016

509 Whether the uncounted DON portion was caused by active or passive release (e.g.,
510 sloppy feeding, cell death, viral infection, or physiological limitation) remains unclear,
511 and the magnitude of DON release relative to the total N uptake remains undetermined,
512 even though a handful of studies have revealed its significance (Bronk and Glibert,
513 1993; Bronk and Steinberg, 2008; Sipler and Bronk, 2015). More experiments are
514 required to explore the importance of this uncounted portion in field studies.
515 Nevertheless, our results from the mass balance and matrix solution suggest the
516 significance of DON release, regardless of the nutrient status.

517 On the other hand, the end products of ammonium oxidation or nitrification are
518 consumed by phytoplankton continuously, particularly in a euphotic layer full of
519 photosynthetic autotrophs. In many cases, nitrate uptake occurs in both light and dark
520 conditions (e.g. Dugdale and Goering, 1967; Lipschultz, 200); Mulholland and Lomas,
521 2008). The significant consumption of end products (NO_2^- and NO_x^-) may bias the
522 conventional rate calculation. We can clearly see that possibility in Eq. (19). Even
523 though the consumption of NO_x^- results in a net decreasing trend of $^{15}NO_x^-$ (Figs. 2r
524 and 4n), the NH_4^+ oxidation/nitrification rate in both the WYW and WNP cases could
525 be obtained (see Table 3) as long as r_{NOx-} was increasing (i.e., positive $(r_t - r_0)$ in Eq.
526 (19)). The NH_4^+ oxidation/nitrification rate in the high- and low-nutrient cases (0.41
527 and 0.046 nmol L^{-1} h^{-1}, respectively) derived from the canonical method were lower
528 than those (0.90 and 0.051 nmol L^{-1} h^{-1}, respectively) from the matrix method. This
529 apparent discrepancy resulted from product consumption. In fact, Santoro et al. (2010a,

Biogeosciences Discuss., doi:10.5194/bg-2016-298, 2016
Manuscript under review for journal Biogeosciences
Published: 2 August 2016

530 2013) realized the effect of consumption on their rate calculation. To overcome this
531 consumption effect induced by the first-order reaction, they took NO_x^- removal into
532 consideration and formulated a new equation, a function of nitrification rate (F) and
533 NO_x^- uptake rate (k). Following Santoro et al. (2010a), we calculated the nitrification
534 rate for the low-nutrient case (via a nonlinear least-squares curve-fitting routine in
535 Matlab by using the first three time points of the $^{15}N_{NOx-}/^{14}N_{NOx-}$ measurements) to be
536 0.056 nmol L^{-1} h^{-1} (Table 3), which was slightly (~10%) larger than the matrix-derived
537 rate (0.051 nmol L^{-1} h^{-1}). The simulations of $\delta^{15}NO_x^-$ and r_{NOx-} deduced from results by
538 the method of Santoro et al. (2010a) agreed well with the isotope matrix method (Figs.
539 5 j and n). Interestingly, their nitrate uptake rate (k = 0.010 h^{-1}) was only one-sixth that
540 (0.059 h^{-1}) derived from the matrix method, although a comparable nitrification rate
541 was obtained when the consumption term was taken into account. Surprisingly, when
542 we introduced the two parameters to generate the time courses of the $^{15}NO_x^-$, $^{14}NO_x^-$,
543 and NO_x^- concentrations, we found much slower decreasing trends in the
544 concentrations (Figs. 5 b, f, and r). In fact, the formula produced by Santoro et al.
545 (2010a) is constrained only by the ratio changes rather than the individual
546 concentration changes in $^{15}NO_x^-$ and $^{14}NO_x^-$. Thus, the nonlinear curve-fitting method
547 by Matlab may only provide a correct simulation for the ratio change. This implies that
548 the nitrate uptake rate derived from the non-linear curve-fitting method in Matlab
549 should be validated by using the concentration of nitrate at the end point, as was done

Biogeosciences Discuss., doi:10.5194/bg-2016-298, 2016
Manuscript under review for journal Biogeosciences
Published: 2 August 2016

by Santoro et al (2013). Thus, a precise measurement of concentration changes is vital in time series incubations for nitrification.

To evaluate the fractional contribution of nitrification to NO_3^- uptake as done by Yool et al. (2007), labeled $^{15}NH_4^+$ and $^{15}NO_3^-$ addition were needed in parallel incubations; meanwhile, a realistic evaluation can be achieved only when the incubation is conducted in the same bottle under *in situ* light conditions, in which light inhibition and substrate competition must occur simultaneously. The isotope matrix method is so far the most convenient and suitable method for evaluating the relative importance of co-occuring nitrification and new production. Through the matrix, the contributions of nitrification to new production were approximately 0.4 % and 0.2 % in the high- and low-nutrient cases, respectively; these relatively low values were probably due to the light inhibition effects on nitrifiers.

Another example is resolution of the mechanisms of formation of the primary nitrite maximum (PNM). Previous studies have involved addition of various tracers into parallel incubation bottles to determine associated individual processes (Olson, 1981a, 1981b; Lomas and Lipschultz, 2006; Santoro et al., 2013). However, this laboursome operation does not exclude the dynamic N interactions. Furthermore, the matrix method is also appropriate for probing the effects of environmental factors (e.g., CO_2, pH, temperature, light intensity, and dissolved oxygen) on the interactive N processes in one single incubation bottle. For example, after synthesizing studies of CO_2 effects

Biogeosciences Discuss., doi:10.5194/bg-2016-298, 2016
Manuscript under review for journal Biogeosciences
Published: 2 August 2016

570 on N_2-fixation, nitrification, and denitrification, Hutchins et al. (2009) indicated that
571 the N cycle may strongly respond to higher CO_2. By labeling one N species and
572 controlling the level of CO_2, our isotope matrix method can determine these rates
573 simultaneously. Thus, a better evaluation of the response of the N cycle to rising CO_2
574 can be achieved.

575 **6. Conclusion**

576 Although the assessment of relevant errors is weakened due to the involvement of
577 different error sources (analytical error, error propagation in calculation, and matrix
578 solution error), and the estimate of uncertainty for this isotope matrix method is not a
579 simple statistical question, the isotope matrix method saves both labor and time in the
580 field if one intends to obtain multiple rates simultaneously. Given the progress in
581 analytical techniques used to measure the concentration and isotopic composition of
582 nitrogen species, the isotope matrix method presents a promising avenue for the study
583 of rates of nitrogen processes with a system-wide perspective.

584 **Acknowledgement**

585 We sincerely thank Wenbin Zou and Tao Huang at the State Key Laboratory of Marine
586 Environmental Science (Xiamen University, China) for their valuable help with the
587 water sampling and the on-board trace NH_4^+ concentration analysis during the 2015
588 NWP cruise. This research was funded by the National Natural Science Foundation of
589 China (NSFC U1305233, 2014CB953702, 91328207, 2015CB954003).

Biogeosciences Discuss., doi:10.5194/bg-2016-298, 2016
Manuscript under review for journal Biogeosciences
Published: 2 August 2016

590 **References**

591 Beman, J. M., Popp, B. N., and Alford, S. E.: Quantification of ammonia oxidation
592 rates and ammonia-oxidizing archaea and bacteria at high resolution in the Gulf of
593 California and eastern tropical North Pacific Ocean, Limnol. Oceanogr., 57, 711-726,
594 doi:10.4319/lo.2012.57.3.0711, 2012.
595 Bianchi, M., Feliatra, F., Tréguer, P., Vincendeau, M.-A., and Morvan, J.:
596 Nitrification rates, ammonium and nitrate distribution in upper layers of the water
597 column and in sediments of the Indian sector of the Southern Ocean, Deep Sea Res.
598 Part II: Top. Stud. Oceanogr., 44, 1017-1032, doi:10.1016/S0967-0645(96)00109-9,
599 1997.
600 Braman, R. S., and Hendrix, S. A.: Nanogram nitrite and nitrate determination in
601 environmental and biological materials by vanadium (III) reduction with
602 chemiluminescence detection, Anal. Chem., 61, 2715-2718, doi:
603 10.1021/ac00199a007, 1989.
604 Bronk, D., and Ward, B. B.: Gross and net nitrogen uptake and DON release in the
605 euphotic zone of Monterey Bay, California, Limnol. 0ceanogr., 44, 573-585, 1999.
606 Bronk, D., and Ward, B. B.: Inorganic and organic nitrogen cycling in the Southern
607 California Bight, Deep Sea Res. Part I Oceanogr. Res. Pap., 52, 2285-2300,
608 doi:10.1016/j.dsr.2005.08.002, 2005.
609 Bronk, D., Killberg-Thoreson, L., Sipler, R., Mulholland, M., Roberts, Q., Bernhardt,
610 P., Garrett, M., O'Neil, J., and Heil, C.: Nitrogen uptake and regeneration (ammonium
611 regeneration, nitrification and photoproduction) in waters of the West Florida Shelf
612 prone to blooms of Karenia brevis, Harmful Algae, 38, 50-62,
613 doi:10.1016/j.hal.2014.04.007, 2014.
614 Bronk, D. A., and Glibert, P. M.: Contrasting patterns of dissolved organic nitrogen
615 release by two size fractions of estuarine plankton during a period of rapid NH_4^+
616 consumption and NO_2^- production, Mar. Ecol. Prog. Ser., 96, 291-291, 1993.
617 Bronk, D. A., Glibert, P. M., and Ward, B. B.: Nitrogen uptake, dissolved organic
618 nitrogen release, and new production, Science, 265, 1843-1846, 1994.
619 Bronk, D. A., and Ward, B. B.: Magnitude of dissolved organic nitrogen release
620 relative to gross nitrogen uptake in marine systems, Limnol. Oceanogr., 45,
621 1879-1883, doi: 10.4319/lo.2000.45.8.1879, 2000.
622 Bronk, D. A., and Steinberg, D. K.: Nitrogen regeneration, in Nitrogen in the Marine
623 Environment, edited by: Capone, D. A., Bronk, D. A., Mulholland, M. R., Carpenter,
624 E. J., Academic Press, London, U.K., 385-467, 2008.
625 Casciotti, K., Sigman, D., Hastings, M. G., Böhlke, J., and Hilkert, A.: Measurement
626 of the oxygen isotopic composition of nitrate in seawater and freshwater using the
627 denitrifier method, Anal. Chem., 74, 4905-4912, 2002.
628 Casciotti, K. L.: Nitrogen and Oxygen Isotopic Studies of the Marine Nitrogen Cycle,
629 Ann. Rev. Mar. Sci., 8, 379-407, doi: 10.1146/annurev-marine-010213-135052,
630 2016.

631 Chen, Y.-l. L.: Spatial and seasonal variations of nitrate-based new production and
632 primary production in the South China Sea, Deep Sea Res. Part I Oceanogr. Res. Pap.,
633 52, 319-340, doi:10.1016/j.dsr.2004.11.001, 2005.
634 Clark, D. R., Fileman, T. W., Joint, I.: Determination of ammonium regeneration rates
635 in the oligotrophic ocean by gas chromatography/mass spectrometry. Mar. Chem.,
636 98(2-4),121-130, doi: 10.1016/j.marchem.2005.08.006, 2006.
637 Collos, Y.: Nitrate uptake, nitrite release and uptake, and new production estimates,
638 Mar. Ecol. Prog. Ser., 171, 293-301, doi:10.3354/meps171293, 1998.
639 Daims, H., Lebedeva, E. V., Pjevac, P., Han, P., Herbold, C., Albertsen, M., Jehmlich,
640 N., Palatinszky, M., Vierheilig, J., Bulaev, A., Kirkegaard, R. H., von Bergen, M.,
641 Rattei, T., Bendinger, B., Nielsen, P. H., and Wagner, M.: Complete nitrification by
642 Nitrospira bacteria, Nature, 528, 504-509, 10.1038/nature16461,
643 doi:10.1038/nature16461, 2015.
644 Dickson, M.-L., and Wheeler, P. A.: Ammonium uptake and regeneration rates in a
645 coastal upwelling regime, Mar. Ecol. Prog. Ser., 121, 239-248, 1995.
646 Dugdale, R., and Goering, J.: Uptake of new and regenerated forms of nitrogen in
647 primary productivity, Limnol. Oceanogr., 12, 196-206, DOI:
648 10.4319/lo.1967.12.2.0196, 1967.
649 Dugdale, R., and Wilkerson, F.: The use of ^{15}N to measure nitrogen uptake in
650 eutrophic oceans; experimental considerations, Limnol. Oceanogr., 31, 673-689, doi:
651 10.4319/lo.1986.31.4.0673, 1986.
652 Falkowski, P. G.: Evolution of the nitrogen cycle and its influence on the biological
653 sequestration of CO_2 in the ocean, Nature, 387, 272-275, doi: 10.1038/387272a0,
654 1997.
655 Fernandez, C., and Farías, L.: Assimilation and regeneration of inorganic nitrogen in a
656 coastal upwelling system: ammonium and nitrate utilization, Mar. Ecol. Prog. Ser.,
657 451, 1-14, doi:10.3354/meps09683, 2012.
658 Flynn, K., and Flynn, K.: Release of nitrite by marine dinoflagellates: development of
659 a mathematical simulation, Mar. Biol., 130, 455-470, doi: 10.1007/s002270050266,
660 1998.
661 Gilbert, P. M., Lipschultz, F., McCarthy, J. J., and Altabet, M. A.: Isotope dilution
662 models of uptake and remineralization of ammonium by marine plankton, Limnol.
663 Oceanogr., 27, 639-650, 1982.
664 Granger, J., and Sigman, D. M.: Removal of nitrite with sulfamic acid for nitrate N
665 and O isotope analysis with the denitrifier method, Rapid Commun. Mass Spectrom.,
666 23, 3753-3762, 10.1002/rcm.4307, doi: 10.1002/rcm.4307, 2009.
667 Grundle, D. S., and Juniper, S. K.: Nitrification from the lower euphotic zone to the
668 sub-oxic waters of a highly productive British Columbia fjord, Mar. Chem., 126,
669 173-181, doi:10.1016/j.marchem.2011.06.001, 2011.
670 Grundle, D. S., Juniper, S. K., and Giesbrecht, K. E.: Euphotic zone nitrification in
671 the NE subarctic Pacific: Implications for measurements of new production, Mar.
672 Chem., 155, 113-123, doi:10.1016/j.marchem.2013.06.004, 2013.

673 Hannon, J. E., and Böhlke, J. K.: Determination of the delta ($^{15}N/^{14}N$) of Ammonium
674 (NH_4^+) in Water: RSIL Lab Code 2898, US Geological Survey 2328-7055, 2008.
675 Harrison, P. J., and Davis, C. O.: Use of the perturbation technique to measure
676 nutrient uptake rates of natural phytoplankton populations, Deep Sea Res., 24,
677 247-255, doi:10.1016/S0146-6291(77)80003-9, 1977.
678 Harvey, W. A., and Caperon, J.: The rate of utilization of urea, ammonium, and
679 nitrate by natural populations of marine phytoplankton in a eutrophic environment,
680 Pacific Science, 30 (4), 329-340, http://hdl.handle.net/10125/1169, 1976.
681 Holmes, R., McClelland, J., Sigman, D., Fry, B., and Peterson, B.: Measuring
682 $^{15}N–NH_4^+$ in marine, estuarine and fresh waters: An adaptation of the ammonia
683 diffusion method for samples with low ammonium concentrations, Mar. Chem., 60,
684 235-243, doi:10.1016/S0304-4203(97)00099-6, 1998.
685 Horrigan, S., Carlucci, A., and Williams, P.: Light inhibition of nitrification in
686 sea-surface films [California], J. Mar. Res., 1981.
687 Howard, M. D. A., Cochlan, W. P., Ladizinsky, N., and Kudela, R. M.: Nitrogenous
688 preference of toxigenic Pseudo-nitzschia australis (Bacillariophyceae) from field and
689 laboratory experiments, Harmful Algae, 6, 206-217, doi:10.1016/j.hal.2006.06.003,
690 2007.
691 Hsiao, S.-Y., Hsu, T.-C., Liu, J.-w., Xie, X., Zhang, Y., Lin, J., Wang, H., Yang, J.-Y.,
692 Hsu, S.-C., and Dai, M.: Nitrification and its oxygen consumption along the turbid
693 Chang Jiang River plume, Biogeosciences, 11, 2083-2098,
694 doi:10.5194/bg-11-2083-2014, 2014.
695 Hutchins, D. A., Mulholland, M. R., and Fu, F.: Nutrient cycles and marine microbes
696 in a CO_2-enriched ocean, Oceanography, 2009.
697 Knapp, A. N., Sigman, D. M., and Lipschultz, F.: N isotopic composition of dissolved
698 organic nitrogen and nitrate at the Bermuda Atlantic Time-series Study site, Global
699 Biogeochem. Cycles, 19, doi: 10.1029/2004GB002320, 2005.
700 Koroleff, F.: Simultaneous oxidation of nitrogen and phosphorus compounds by
701 persulfate, Methods of seawater analysis, 2, 205-206, 1983.
702 Lipschultz, F.: A time-series assessment of the nitrogen cycle at BATS, Deep Sea Res.
703 Part II Top. Stud. Oceanogr., 48, 1897-1924, doi:10.1016/S0967-0645(00)00168-5,
704 2001.
705 Lomas, M. W., and Lipschultz, F.: Forming the primary nitrite maximum: Nitrifiers or
706 phytoplankton?, Limnol. Oceanogr., 51, 2453-2467, doi: 10.4319/lo.2006.51.5.2453,
707 2006.
708 MacIsaac, J., and Dugdale, R.: The kinetics of nitrate and ammonia uptake by natural
709 populations of marine phytoplankton, Deep Sea Res. Oceanogr. Abstracts, 45-57,
710 doi:10.1016/0011-7471(69)90049-7, 1969.
711 Marchant, H. K., Mohr, W., Kuypers, M. M. M.: Recent advances in marine N-cycle
712 studies using ^{15}N labeling methods. Curr. Opin. Biotechnol., 41, 53-59,
713 doi:10.1016/j.copbio.2016.04.019, 2016.
714 Martens-Habbena, W., Qin, W., Horak, R. E., Urakawa, H., Schauer, A. J., Moffett, J.
715 W., Armbrust, E. V., Ingalls, A. E., Devol, A. H., and Stahl, D. A.: The production of

716 nitric oxide by marine ammonia-oxidizing archaea and inhibition of archaeal
717 ammonia oxidation by a nitric oxide scavenger, Environ. Microbiol., 17, 2261-2274,
718 10.1111/1462-2920.12677, doi: 10.1111/1462-2920.12677, 2015.
719 McCarthy, J. J., and Eppley, R. W.: A comparison of chemical, isotopic, and
720 enzymatic methods for measuring nitrogen assimilation of marine phytoplankton,
721 Limnol. Oceanogr., 17, 371-382, doi: 10.4319/lo.1972.17.3.0371, 1972.
722 McIlvin, M. R., and Altabet, M. A.: Chemical conversion of nitrate and nitrite to
723 nitrous oxide for nitrogen and oxygen isotopic analysis in freshwater and seawater,
724 Anal. Chem., 77, 5589-5595, doi: 10.1021/ac050528s, 2005.
725 Merbt, S. N., Stahl, D. A., Casamayor, E. O., Martí, E., Nicol, G. W., and Prosser, J.
726 I.: Differential photoinhibition of bacterial and archaeal ammonia oxidation, FEMS
727 Microbiol. Lett., 327, 41-46, doi: http://dx.doi.org/10.1111/j.1574-6968.2011.02457.x,
728 2012.
729 Middelburg, J. J., and Nieuwenhuize, J.: Uptake of dissolved inorganic nitrogen in
730 turbid, tidal estuaries, Mar. Ecol. Prog. Ser., 192, 79-88, doi:10.3354/meps192079,
731 2000.
732 Mulholland, M. R., and Lomas, M. W.: Nitrogen uptake and assimilation, in Nitrogen
733 in the marine environment, edited by: Capone, D. A., Bronk, D. A., Mulholland, M.
734 R., Carpenter, E. J., Academic Press, London, U.K., 303-384, 2008.
735 Newell, S. E., Babbin, A. R., Jayakumar, A., and Ward, B. B.: Ammonia oxidation
736 rates and nitrification in the Arabian Sea, Global Biogeochem. Cycles, 25, doi:
737 10.1029/2010GB003940, 2011.
738 Newell, S. E., Fawcett, S. E., and Ward, B. B.: Depth distribution of ammonia
739 oxidation rates and ammonia-oxidizer community composition in the Sargasso Sea,
740 Limnol. Oceanogr., 58, 1491-1500, doi:10.4319/lo.2013.58.4.1491, 2013.
741 Olson, R.: N-15 tracer studies of the primary nitrite maximum, J. Mar. Res., 39,
742 203-226, 1981a.
743 Olson, R. J.: Differential photoinhibition of marine nitrifying bacteria: a possible
744 mechanism for the formation of the primary nitrite maximum, J. Mar. Res., 39,
745 227-238, 1981b.
746 Painter, S. C., Patey, M. D., Tarran, G. A., and Torres-Valdés, S.: Picoeukaryote
747 distribution in relation to nitrate uptake in the oceanic nitracline, Aquat. Microb. Ecol.,
748 72, 195-213, doi:10.3354/ame01695, 2014.
749 Pakulski, J., Benner, R., Amon, R., Eadie, B., and Whitledge, T.: Community
750 metabolism and nutrient cycling in the Mississippi River plume: evidence for intense
751 nitrification at intermediate salinities, Mar. Ecol. Prog. Ser., 117, 207, 1995.
752 Peng, X., Fuchsman, C. A., Jayakumar, A., Oleynik, S., Martens‐Habbena, W.,
753 Devol, A. H., and Ward, B. B.: Ammonia and nitrite oxidation in the Eastern Tropical
754 North Pacific, Global Biogeochem. Cycles, 29, 2034-2049, doi:
755 10.1002/2015GB005278, 2015.
756 Peng, X., Fuchsman, C. A., Jayakumar, A., Warner, M. J., Devol, A. H., and Ward, B.
757 B.: Revisiting nitrification in the eastern tropical South Pacific: A focus on controls, J.
758 Geophys. Res.: Oceans, doi: 10.1002/2015JC011455, 2016.

759 Raimbault, P., and Garcia, N.: Evidence for efficient regenerated production and
760 dinitrogen fixation in nitrogen-deficient waters of the South Pacific Ocean: impact on
761 new and export production estimates, Biogeosciences, 5, 323-338, 2008.
762 Santoro, A., Sakamoto, C., Smith, J., Plant, J., Gehman, A., Worden, A., Johnson, K.,
763 Francis, C., and Casciotti, K.: Measurements of nitrite production in and around the
764 primary nitrite maximum in the central California Current, Biogeosciences, 10,
765 7395-7410, doi:10.5194/bg-10-7395-2013, 2013.
766 Santoro, A. E., Casciotti, K. L., and Francis, C. A.: Activity, abundance and diversity
767 of nitrifying archaea and bacteria in the central California Current, Environ.
768 Microbiol., 12, 1989-2006, doi. L., and Francis, C. A.: Activity, abundance and
769 diversity of nitrifying archaea and bacteria in the central California Current, Environ.
770 Microbiol., 12, 1989-2006, 2010b.
771 Sigman, D., Casciotti, K., Andreani, M., Barford, C., Galanter, M., and Böhlke, J.: A
772 bacterial method for the nitrogen isotopic analysis of nitrate in seawater and
773 freshwater, Anal. Chem., 73, 4145-4153, doi: 10.1021/ac010088e, 2001.
774 Sipler, R. E., and Bronk, D. A.: Dynamics of Dissolved Organic Nitrogen, in
775 Biogeochemistry of Marine Dissolved Organic Matter, edited by: Hansell, D. A.,
776 Carlson, C. A., Academic Press, London, U.K., 127-232, 2015.
777 Smith, J. M., Chavez, F. P., and Francis, C. A.: Ammonium uptake by phytoplankton
778 regulates nitrification in the sunlit ocean, PloS One, 9, e108173, doi:
779 org/10.1371/journal.pone.0108173, 2014.
780 Sunda, W. G., and Ransom, H. D.: Ammonium uptake and growth limitation in
781 marine phytoplankton, Limnol. Oceanogr., 52, 2496–2506, 2007.
782 van Kessel, M. A., Speth, D. R., Albertsen, M., Nielsen, P. H., Opden Camp, H. J.,
783 Kartal, B., Jetten, M. S., and Lucker, S.: Complete nitrification by a single
784 microorganism, Nature, 528, 555-559, 10.1038/nature16459,
785 doi:10.1038/nature16459, 2015.
786 Varela, M. M., Bode, A., Fernandez, E., Gonzalez, N., Kitidis, V., Varela, M., and
787 Woodward, E.: Nitrogen uptake and dissolved organic nitrogen release in planktonic
788 communities characterised by phytoplankton size–structure in the Central Atlantic
789 Ocean, Deep Sea Res. Part I Oceanogr. Res. Pap., 52, 1637-1661,
790 doi:10.1016/j.dsr.2005.03.005, 2005.
791 Wada, E., and Hatton, A.: Nitrite metabolism in the euphotic layer of the central
792 North Pacific Ocean, Limnol. Oceanogr., 16, 766-772, doi:
793 10.4319/lo.1971.16.5.0766 1971.
794 Ward, B. B.: Temporal variability in nitrification rates and related biogeochemical
795 factors in Monterey Bay, California, USA, Mar. Ecol. Prog. Ser., 292, 109,
796 doi:10.3354/meps292097, 2005.
797 Ward, B. B.: Nitrification in marine systems, in Nitrogen in the marine environment,
798 edited by: Capone, D. A., Bronk, D. A., Mulholland, M. R., Carpenter, E. J.,
799 Academic Press, London, U.K., 5, 199-261, 2008.

800 Ward, B. B.: Measurement and distribution of nitrification rates in the oceans, in
801 Methods in enzymology, edited by Abelson, J. N., Simon, M. I., Academic Press,
802 London, U.K., 486, 307-323, 2011.
803 Ward, B. B., Talbot, M., and Perry, M.: Contributions of phytoplankton and nitrifying
804 bacteria to ammonium and nitrite dynamics in coastal waters, Con. Shelf Res., 3,
805 383-398, doi:10.1016/0278-4343(84)90018-9, 1984.
806 Ward, B. B., and Bronk, D.: Net nitrogen uptake and DON release in surface waters:
807 importance of trophic interactions implied from size fractionation experiments, Mar.
808 Ecol. Prog. Ser., 219, 11-24, doi:10.3354/meps219011, 2001.
809 Yool, A., Martin, A. P., Fernández, C., and Clark, D. R.: The significance of
810 nitrification for oceanic new production, Nature, 447, 999-1002,
811 doi:10.1038/nature05885, 2007.
812 Zehr, J. P., and Kudela, R. M.: Nitrogen cycle of the open ocean: from genes to
813 ecosystems, Ann. Rev. Mar. Sci., 3, 197-225, doi:
814 10.1146/annurev-marine-120709-142819, 2011.
815 Zhang, L., Altabet, M. A., Wu, T., and Hadas, O.: Sensitive measurement of NH_4^+
816 $^{15}N/^{14}N$ ($\delta^{15}NH_4^+$) at natural abundance levels in fresh and saltwaters, Anal. Chem.,
817 79, 5297-5303, doi: 10.1021/ac070106d, 2007.
818 Zhu, Y., Yuan, D., Huang, Y., Ma, J., and Feng, S.: A sensitive flow-batch system for
819 on board determination of ultra-trace ammonium in seawater: Method development
820 and shipboard application, Anal. Chim. Acta., 794, 47-54, 10.1016/j.aca.2013.08.009,
821 doi:10.1016/j.aca.2013.08.009, 2013.

822

Biogeosciences Discuss., doi:10.5194/bg-2016-298, 2016
Manuscript under review for journal Biogeosciences
Published: 2 August 2016

Figure Captions

Fig. 1. Model schemes with well-recognized nitrogen transformation processes in high- (a) and low- (b) nutrient aquatic environments. Two pools (inorganic and organic) were categorized (see text). Arrows stand for the transfer flux/rate from the reactant to product pool. The structure and inter-exchanges in the low-nutrient case (Fig. 1 b) are the same as in (a), except that NO_2^- and NO_3^- are combined into NO_x^-.

Fig. 2. Time courses of (a) $[NH_4^+]$, (b) $[NO_2^-]$, (c) $[NO_3^-]$, (d) [PN], (e) [DON], (f) $\delta^{15}N\text{-}NH_4^+$, (g) $\delta^{15}N\text{-}NO_2^-$, (h) $\delta^{15}N\text{-}NO_3^-$, (i) $\delta^{15}N$-PN, (j) $\delta^{15}N$-DON, (k) r_{NH4+}, (l) r_{NO2-}, (m) r_{NO3-}, (n) r_{PN}, (o) r_{DON}, (p) $[^{15}NH_4^+]$, (q) $[^{15}NO_2^-]$, (r) $[^{15}NO_3^-]$, (s) [^{15}N-PN], (t) [^{15}N-DON], (u) $[^{14}NH_4^+]$, (v) $[^{14}NO_2^-]$, (w) $[^{14}NO_3^-]$, (x) [^{14}N-PN] and (y) [^{14}N-DON] during the incubation in the high nutrient case. Data in the plots with grey backgrounds were obtained by mass conservation under the assumption of no NH_4^+ regeneration.

Fig. 3. STELLA-derived and observed values in the high-nutrient case for (a) $[^{15}NH_4^+]$, (b) $[^{15}NO_2^-]$, (c) $[^{15}NO_3^-]$, (d) [^{15}N-PN], (e) [^{15}N-DON], (f) $[^{14}NH_4^+]$, (g) $[^{14}NO_2^-]$, (h) $[^{14}NO_3^-]$, (i) [^{14}N-PN], (j) [^{14}N-DON], (k) r_{NH4+}, (l) r_{NO2-}, (m) r_{NO3-}, (n) r_{PN}, (o) r_{DON}, (p) $\delta^{15}N\text{-}NH_4^+$, (q) $\delta^{15}N\text{-}NO_2^-$, (r) $\delta^{15}N\text{-}NO_3^-$, (s) $\delta^{15}N$-PN, (t) $\delta^{15}N$-DON, (u) $[NH_4^+]$, (v) $[NO_2^-]$, (w) $[NO_3^-]$ (x) [PN] and (y) [DON]. The black open triangles represent the observational values; the black solid line indicate the STELLA model simulation under constant r_{NH4+}; and the green, blue, magenta and pink lines represent the simulations of 1%, 10%, 20% and 50% decreases in r_{NH4+}, respectively.

Biogeosciences Discuss., doi:10.5194/bg-2016-298, 2016
Manuscript under review for journal Biogeosciences
Published: 2 August 2016

843 **Fig.4.** Time courses of (a) [NH_4^+], (b) [NO_x^-], (c) [PN] (d) [DON], (e) δ^{15}N-NH_4^+, (f)
844 δ^{15}N-NO_x^-, (g) δ^{15}N-PN, (h) δ^{15}N-DON, (i) r_{NH4+}, (j) r_{NOx-}, (k) r_{PN}, (l) r_{DON}, (m)
845 [$^{15}NH_4^+$], (n) [$^{15}NO_x^-$], (o) [^{15}N-PN], (p) [^{15}N-DON], (q) [$^{14}NH_4^+$], (r) [$^{14}NO_x^-$], (s)
846 [^{14}N-PN] and (t) [^{14}N-DON] during the incubation in the low-nutrient case. Data in the
847 plots with grey backgrounds were obtained under the assumption of no NH_4^+
848 regeneration. Error bars were shown also in plots and in many cases errors are smaller
849 than the size of the symbols.

850 **Fig. 5.** STELLA-derived and observed values in the low-nutrient case for (a) [$^{15}NH_4^+$],
851 (b) [$^{15}NO_x^-$], (c) [^{15}N-PN], (d) [^{15}N-DON], (e) [$^{14}NH_4^+$], (f) [$^{14}NO_x^-$], (g) [^{14}N-PN], (h)
852 [^{14}N-DON], (i) r_{NH4+}, (j) r_{NOx-}, (k) r_{PN}, (l) r_{DON}, (m) δ^{15}N-NH_4^+, (n) δ^{15}N-NO_x^-, (o)
853 δ^{15}N-PN, (p) δ^{15}N-DON, (q) [NH_4^+], (r) [NO_x^-], (s) [PN] and (t) [DON]. The black
854 open triangles represent the observed values; the black solid lines indicate the
855 STELLA model simulation under constant r_{NH4+}; and the green, blue, magenta and
856 pink lines stand for simulations of 1%, 10%, 20% and 50% decreases in r_{NH4+},
857 respectively. The dashed lines in (b), (f), (j), (n) and (r) were generated from nonlinear
858 least-squares curve-fitting by Matlab following Santoro et al. (2010).
859

Biogeosciences Discuss., doi:10.5194/bg-2016-298, 2016
Manuscript under review for journal Biogeosciences
Published: 2 August 2016

860 **Table Captions**

861 **Table 1.** The matrix results for the rates of N processes in the high-nutrient case under
862 different r_{NH4+} variation conditions.

863 **Table 2.** The matrix results for the specific rates of N processes in the low-nutrient case
864 during the time series incubation.

865 **Table 3.** Comparison of the NH_4^+/ NO_x^- uptake and NH_4^+ oxidation/nitrification rate
866 calculations by the matrix and conventional methods.

867

Biogeosciences Discuss., doi:10.5194/bg-2016-298, 2016
Manuscript under review for journal Biogeosciences
Published: 2 August 2016

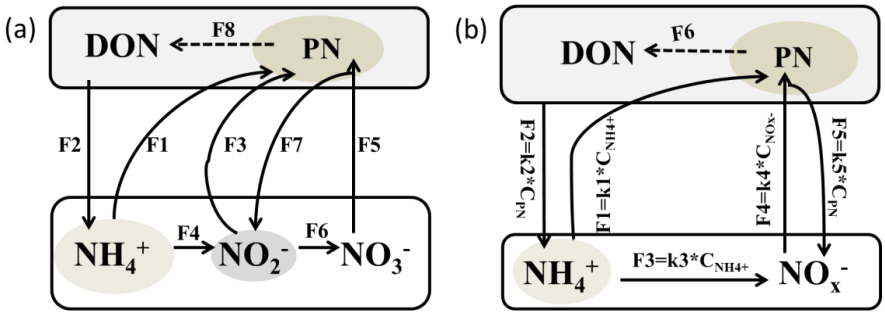

868

869

870 **Figure 1**

871

Biogeosciences Discuss., doi:10.5194/bg-2016-298, 2016
Manuscript under review for journal Biogeosciences
Published: 2 August 2016

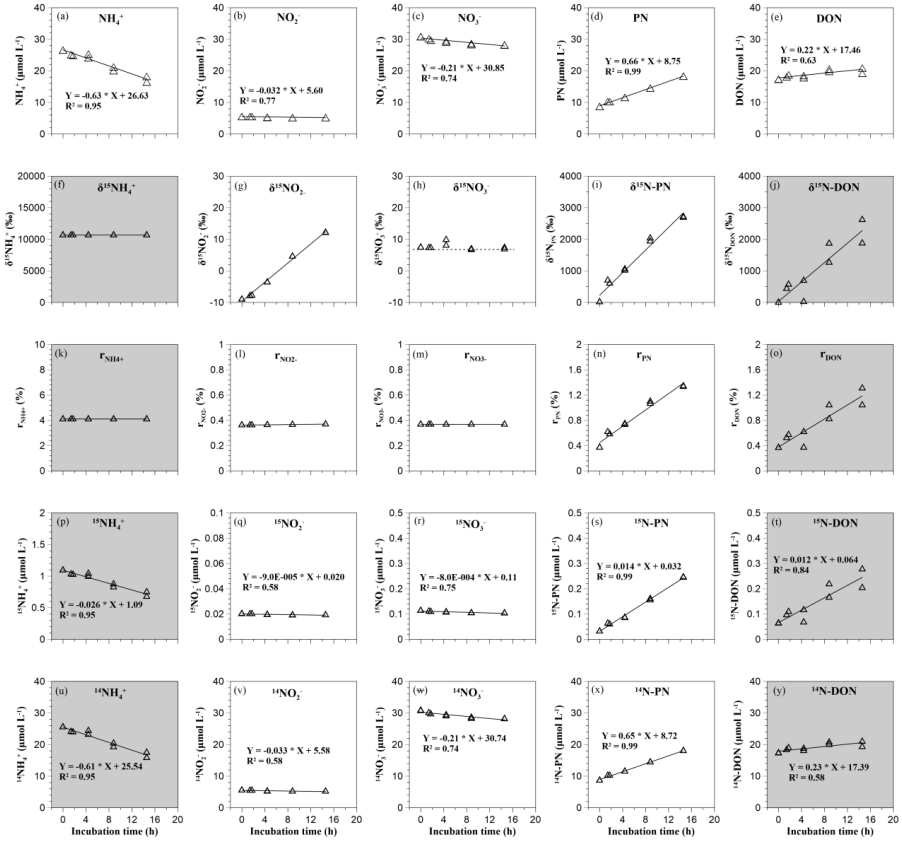

872

873

874 **Figure 2**

875

Biogeosciences Discuss., doi:10.5194/bg-2016-298, 2016
Manuscript under review for journal Biogeosciences
Published: 2 August 2016

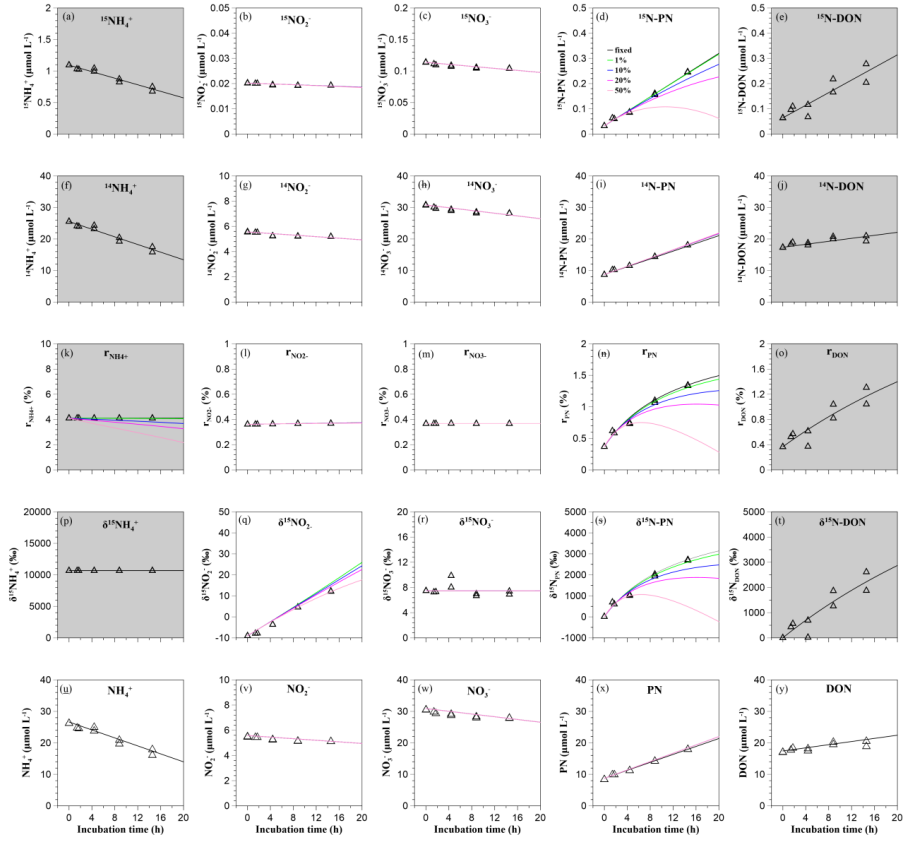

Figure 3

Biogeosciences Discuss., doi:10.5194/bg-2016-298, 2016
Manuscript under review for journal Biogeosciences
Published: 2 August 2016

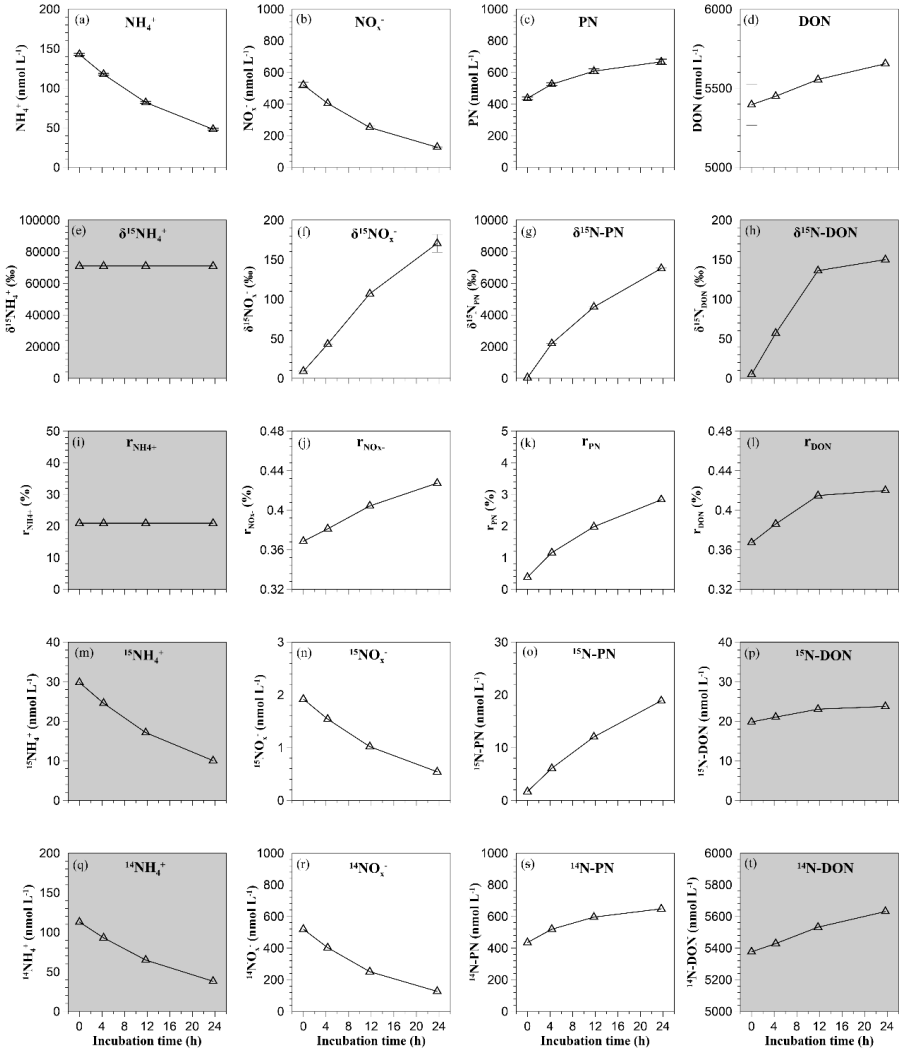

Figure 4

Biogeosciences Discuss., doi:10.5194/bg-2016-298, 2016
Manuscript under review for journal Biogeosciences
Published: 2 August 2016

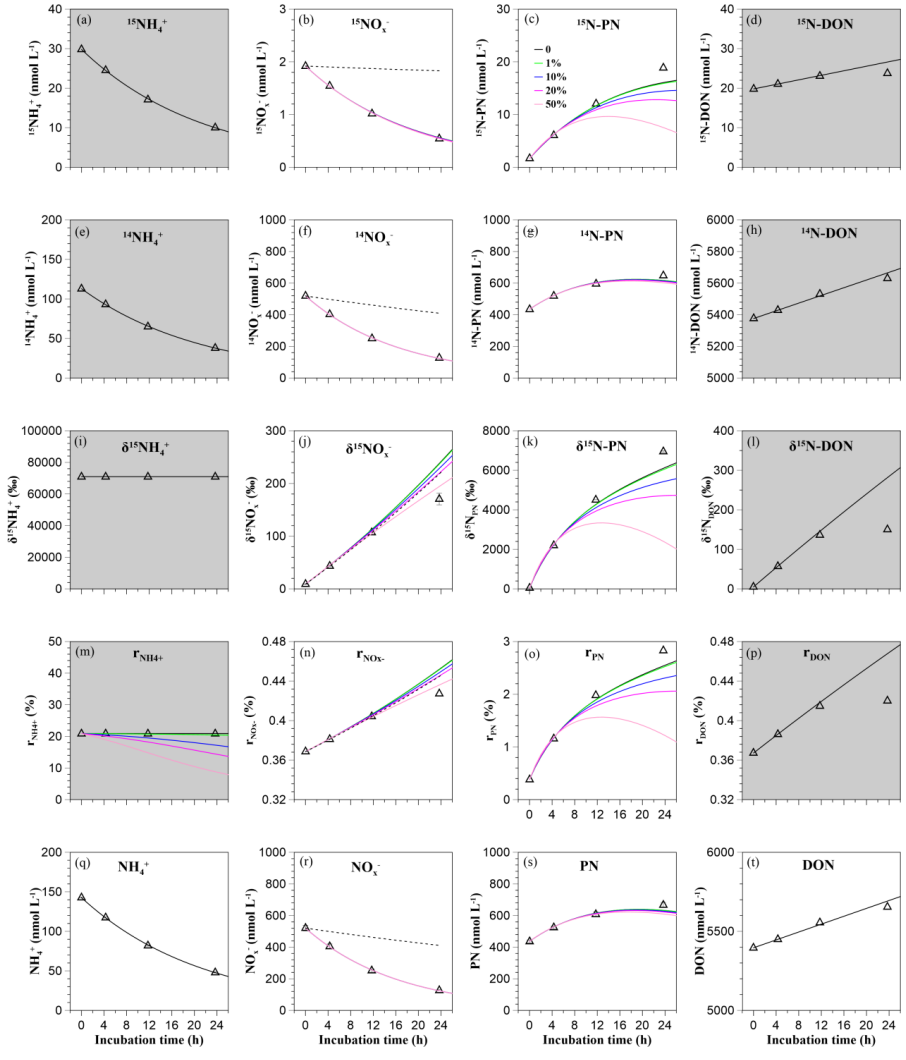

884

885

886 **Figure 5**

887

Biogeosciences Discuss., doi:10.5194/bg-2016-298, 2016
Manuscript under review for journal Biogeosciences
Published: 2 August 2016

888 **Table 1**

r_{NH4+} Decrease* (%)	F1 NH_4^+ uptake	F2 NH_4^+ regeneration	F3 NO_3^- uptake	F4 NH_4^+ oxidation	F5 NO_3^- uptake	F6 NO_2^- oxidation	F7 NO_2^- release	F8 DON release
	μmol L^{-1} h^{-1}							
0	0.63	0	0.032	0.00090	0.22	0	0	0.25
1%	0.65	0.014	0.032	0.00090	0.22	0	0	0.22
10%	0.78	0.15	0.032	0.00090	0.22	0	0	0.22
20%	0.94	0.30	0.032	0.00091	0.22	0	0	0.22
50%	1.41	0.77	0.032	0.00093	0.22	0	0	0.22

889 *The r_{NH4+} decrease (%) represents the total change in r_{NH4+} to the end of the incubation

890 (14.6 h)

891

Biogeosciences Discuss., doi:10.5194/bg-2016-298, 2016
Manuscript under review for journal Biogeosciences
Published: 2 August 2016

892 **Table 2**

r_{NH4+} decrease (%)	k1 NH_4^+ uptake	k2 NH_4^+ regeneration	k3 Nitrification h^{-1}	k4 NO_x^- uptake	k5 NO_x^- release
0	0.045	0	0.00050	0.059	0
1%	0.045	0.00012	0.00050	0.059	0
10%	0.049	0.0012	0.00050	0.059	0
20%	0.054	0.0024	0.00051	0.059	0
50%	0.067	0.0062	0.00052	0.059	0

893

894

Biogeosciences Discuss., doi:10.5194/bg-2016-298, 2016
Manuscript under review for journal Biogeosciences
Published: 2 August 2016

895 **Table 3**

Case	Time (h)	Process	Matrix method (this study)	Traditional rate calculation (nmol L^{-1} h^{-1})	Santoro et al.[13] (2010)*
WYW	0-1.6	NH_4^+ uptake	632.2	413.6	-
WNP	0-4.3	NH_4^+ uptake	4.58*	3.86 *	-
WYW	0-1.6	NH_4^+ oxidation	0.90	0.41	-
WNP	0-4.3	Nitrification	0.051*	0.046*	0.056*[#]
WNP	0-4.3	NO_x^- uptake	0.059*	-	0.01*[$]

896 [*] First-order reaction; [#] F value by Matlab; [$] k value by Matlab.